

---

# A TWO-STAGE APPROACH TO HEAT-MORTALITY RISK ASSESSMENT COMPARING MULTIPLE EXPOSURE-TO-TEMPERATURE MODELS: THE CASE STUDY IN LAZIO, ITALY

---

**Emiliano Ceccarelli**

Department of Statistical Sciences  
Sapienza University of Rome  
Piazzale Aldo Moro, 5  
00185, Rome, Italy

**Jorge Castillo-Mateo**

Department of Statistical Methods and IUMA  
University of Zaragoza  
Pedro Cerbuna 12  
50009, Zaragoza, Spain

**Sandra Gudžiūnaitė**

MRC Centre for Environment and Health  
Department of Epidemiology and Biostatistics  
Imperial College London  
White City Campus  
W12 0BZ, London, UK

**Giada Minelli**

Statistical Services  
Istituto Superiore di Sanità  
Viale Regina Elena, 299  
00161, Rome, Italy

**Giovanna Jona Lasino**

Department of Statistical Sciences  
Sapienza University of Rome  
Piazzale Aldo Moro, 5  
00185, Rome, Italy

**Marta Blangiardo**

MRC Centre for Environment and Health  
Department of Epidemiology and Biostatistics  
Imperial College London  
White City Campus  
W12 0BZ, London, UK

December 17, 2025

## ABSTRACT

This study investigates how different spatiotemporal temperature models affect the estimation of heat-related mortality in Lazio, Italy (2008–2022). First, we compare three methods to reconstruct daily maximum temperature at the municipality level: 1. a Bayesian quantile regression model with spatial interpolation, 2. a Bayesian Gaussian regression model, 3. the gridded reanalysis data from ERA5-Land. Both Bayesian models are station-based and exhibit higher and more spatially variable temperatures compared to ERA5-Land. Then, using individual mortality data for cardiovascular and respiratory causes, we estimate temperature-mortality associations through Bayesian conditional Poisson models in a case-crossover design. Exposure is defined as the mean maximum temperature over the previous three days. Additional models include heatwave definitions combining different thresholds and durations. All models exhibit a marked increase in relative risk at high temperatures; however, the temperature of minimum risk varies significantly across methods. Stratified analyses reveal higher relative risk increases in females and the elderly (80+). Heatwave effects depend on the definitions used, but all methods capture an increased mortality risk associated with prolonged heat exposure. Results confirm the importance of temperature model choice in epidemiology and provide insights for early warning systems and climate-health adaptation strategies.

**Keywords** Bayesian hierarchical modelling, Heat, Human health, Mortality, Quantile regression

## 1 Introduction

The impact of high temperatures on human health is a well-established public health concern, with numerous studies linking both heat and cold exposure to increased mortality, particularly from cardiovascular and respiratory causes (Barnett, 2007; Baccini et al., 2008; Gasparrini et al., 2015). In the context of climate change, heat-related health risks are expected to become more severe, as both the frequency and intensity of extreme temperature events are projected to increase in the coming decades (Alfano et al., 2023). While the adverse effects of extreme heat are now well recognized, discussion follows on the optimal temperatures that correspond to minimum effects for various health outcomes, which vary for different regions of the World and depend on the temperature database considered.

The effect of heat is typically investigated by regressing death counts within a time frame (usually weeks or days) against a respective measure of temperature (e.g. average or maximum) on a continuous scale. An alternative way to define heat exposure is through the concept of heatwaves, which are periods of multiple consecutive days in which temperatures surpass a certain threshold (Robinson, 2001; Perkins and Alexander, 2013). It has been hypothesized that exposure to multiple consecutive hot days may constitute a health risk in addition to daily temperature alone (Gasparrini and Armstrong, 2011). Indeed, the physiological and behavioral mechanisms for thermo-regulation are prone to exhaustion and ultimately failure among the most vulnerable populations (e.g. the elderly and those living with chronic conditions) (Bennett et al., 2014; Blum et al., 2025). Hence, a way to account for this is to add a categorical variable indicating heatwave days to test whether it captures some variations in health outcomes other than continuous temperature alone (Robinson, 2001). This study will employ both methods for testing the effects of heat on mortality.

Most epidemiological studies rely on gridded satellite-based reanalysis data products, also called gridded climate datasets (GCDs), such as Copernicus' ERA5-Land (Muñoz-Sabater et al., 2021; Copernicus Climate Change Service, 2023), to assess the dose-response association between heat and health (Ballester et al., 2023; Ceccarelli et al., 2024). GCDs are easily accessible and provide a large temporal coverage, but are also prone to measurement error in complex terrains such as coastal areas, affected by mixed land-sea pixels, or mountainous regions, characterized by large elevation differences; this can affect the accuracy of local temperature estimates (Donat et al., 2014). Many argue that ground-based weather stations should be preferred since they provide direct and precise observations at specific locations (Mendelsohn et al., 2007; Colston et al., 2018). However, weather stations are often unevenly distributed, with denser coverage in highly populated areas and in more developed regions. These differences in spatial resolution, representativeness, and data-generating processes can result in different exposure estimates at the local scale (Sheridan et al., 2020; McNicholl et al., 2021), especially for spatially heterogeneous regions. In turn, such discrepancies can lead to differences in estimated health risks, with important public health implications, for instance around early warning systems for high temperatures.

The spatial scale of the temperature data plays a crucial role, since it should align with the resolution of the health data, commonly available at the municipality level. While ERA5-Land provides a relatively high resolution of 9 km (Muñoz-Sabater et al., 2021), this is still insufficient to capture fine-scale temperature variability between neighbouring municipalities, especially in geographically complex regions. In contrast, station-based data can offer highly localized information, but their spatial distribution is inconsistent, depending on factors like population density and geography. This often results in clusters of stations in urban centers and a lack of coverage in rural or mountainous zones.

In literature, temperature estimates derived from ground-based monitoring stations can be effectively interpolated through spatiotemporal statistical models. For instance, Benavides et al. (2007) uses a kriging approach comparing several geostatistical and regression-based methods in a mountainous region of northern Spain. Craigmire and Guttorm (2011), Verdin et al. (2015), and Castillo-Mateo et al. (2022) developed spatiotemporal hierarchical Bayesian models. In particular, Craigmire and Guttorm (2011) estimated daily mean temperatures in Central Sweden using wavelet-based trend components, while Verdin et al. (2015) and Castillo-Mateo et al. (2022) modelled minimum and/or maximum temperatures in the Pampas region of Argentina and the Aragón region of Spain, respectively, incorporating autoregressive structures and spatial Gaussian processes. In a similar context, quantile regression (Koenker and Bassett Jr, 1978; Koenker, 2005), and quantile autoregression (Koenker and Xiao, 2006), have been used extensively to model extreme temperatures, both in a Frequentist (Gao and Franzke, 2017) and Bayesian approach (Ferraz Do Nascimento and Bourguignon, 2020; Castillo-Mateo et al., 2023). Yet, a comprehensive comparison between quantile regression methods and traditional geostatistical models for modelling high temperatures remains unexplored.

In this context, the present study aims to compare three different spatiotemporal approaches to estimate daily maximum temperatures at high spatiotemporal resolution: a benchmark satellite-based method (ERA5-Land), and two station-based approaches that can account for covariates (e.g. altitude) or are tailored to model high quantiles of the temperature distribution. We then assess how the differences in the estimated temperatures using these three methods lead to differences in the estimated temperature-mortality associations.

The first approach is based on the Bayesian spatial quantile autoregressive model by Castillo-Mateo et al. (2023), which models different parts of the temperature distribution, with a particular focus on high quantiles. The second approach adopts a Bayesian geostatistical framework, widely applied in environmental exposure modelling such as air pollution studies (Cameletti et al., 2013). Both of these approaches rely on ground-based monitoring stations as input data. The third approach, by contrast, uses GCD from ERA5-Land, a satellite-based product commonly employed in epidemiological practice due to its accessibility and broad temporal coverage (Ballester et al., 2023; Ceccarelli et al., 2024).

Most literature on the temperature-mortality association uses aggregated data at the city or regional level (Barnett, 2007; Royé et al., 2020), whilst a limited number of studies rely on individual-level information. In both cases, the temperature-mortality association is known to be non-linear, usually modelled with splines (Armstrong et al., 2011), to obtain what are often described as U-, V-, or J-shaped relationships (Braga et al., 2002). Use of individual data allows investigation of possible effect modification by individual factors, and it avoids ecological bias (Shafran-Nathan et al., 2017). We took advantage of the individual data availability of the outcome and adopted a case-crossover study design, where each case serves as its own control, thus accounting for time-invariant variables like socioeconomic characteristics (Maclure, 1991).

The contributions of this work can be divided into two stages:

1. Spatiotemporal modelling of daily maximum temperatures to estimate an exposure surface to high temperatures;
2. Epidemiological modelling to assess the association between high temperatures and cause-specific mortality.

As a case study, we use the Lazio region in Italy for the period covering 2008 to 2022 at the municipality level. Analyses are restricted to the summer months, the warmer part of the year. Italy is one of the European countries most vulnerable to the effects of climate change, with projections indicating a marked increase in the frequency, duration, and intensity of extreme heat events in the coming decades (de' Donato et al., 2019). Within this national context, the Lazio region, located in central Italy, offers a particularly interesting case study due to its diverse geography and population distribution. The region includes mountainous areas in the Apennines, extensive coastal zones along the Tyrrhenian Sea and several lakes, for a total land area of 17,242 km<sup>2</sup>. The capital city of the country, Rome, is located in the region, and this offers the possibility to study a mix of densely populated urban centers and more rural areas. The region is home to 5,714,882 inhabitants, 2,746,984 of which live in the municipality of Rome.

The rest of the paper is structured as follows. Section 2 presents the data sources used, the three methods for estimating the temperature surface, and the epidemiological model. Section 3 describes the models' estimates, and Section 4 ends the paper with the conclusions and future work. Supplementary Materials accompanying this paper appear online.

## 2 Data and methods

### 2.1 Data sources

All analyses are restricted to the Lazio region of Italy; see Figure S1 of the Supplementary Materials. The study period spans from 1-1-2008 to 31-12-2022, reflecting the availability of consistent monitoring data; the analyses are restricted to the warm months: May to September in the first stage, to capture the broader high-temperature season, and June to August in the second stage, to focus specifically on the summer period.

In the first stage of the analysis, we used two sources of temperature data: (a) the daily maximum temperatures recorded by 222 monitoring stations in the region, provided by the Italian Institute for Environmental Protection and Research (ISPRA); (b) maximum daily temperatures computed from the hourly air temperature at 2 meters above sea level, extracted from the ERA5-Land dataset (Muñoz-Sabater et al., 2021). In addition, we considered the average municipality altitude provided by the Italian National Institute of Statistics (ISTAT).

In the second stage of the analysis, we extracted cause-specific individual mortality records from the ISTAT death certificate archives in the time period under study. We further selected only adult deaths (18+ years) with the underline cause due to diseases of the circulatory system and respiratory system, I00-I99 and J00-J99, based on the International Classification of Diseases (ICD-10) codes (WHO, 2016).

## 2.2 Stage 1: Spatiotemporal model of maximum daily temperature

In this section, we compare three different approaches for estimating municipality-level daily maximum temperatures in the Lazio region, denoted by  $D \subset \mathbb{R}^2$ . For all three methods, we aim to derive point estimates of temperature that will be used as covariates in the second-stage epidemiological models.

### 2.2.1 Method 1: Geospatial quantile regression model

**Spatial quantile autoregression** This approach is based on the Bayesian Geospatial quantile regression model (GQRM) proposed by Castillo-Mateo et al. (2023), for quantile levels  $\tau \in T = \{0.05, 0.10, 0.20, \dots, 0.80, 0.90, 0.95\}$ . Let  $Y_{t\ell}(\mathbf{s})$  denote the daily maximum temperature of day  $\ell$ , year  $t$ , and site  $\mathbf{s} \in D$ . For each quantile level  $\tau$ , we considered the following model:

$$\begin{aligned} Y_{t\ell}(\mathbf{s}) &= Q_{Y_{t\ell}(\mathbf{s})}(\tau \mid Y_{t,\ell-1}(\mathbf{s})) + \epsilon_{t\ell}^\tau(\mathbf{s}) \\ &= q_{t\ell}^\tau(\mathbf{s}) + \rho^\tau(\mathbf{s}) (Y_{t,\ell-1}(\mathbf{s}) - q_{t,\ell-1}^\tau(\mathbf{s})) + \epsilon_{t\ell}^\tau(\mathbf{s}) \end{aligned} \quad (1)$$

where  $Q_{Y_{t\ell}(\mathbf{s})}(\tau \mid Y_{t,\ell-1}(\mathbf{s}))$  is the  $\tau$ -level conditional quantile of  $Y_{t\ell}(\mathbf{s})$  given  $Y_{t,\ell-1}(\mathbf{s})$ , and the error term is assumed to follow an asymmetric Laplace (AL) distribution, as is common in Bayesian quantile regression (Yu and Moyeed, 2001); specifically,  $\epsilon_{t\ell}^\tau(\mathbf{s}) \sim \text{ind. AL}(0, \sigma^\tau(\mathbf{s}), \tau)$ . The spatially varying error scale  $\sigma^\tau(\mathbf{s})$  and autoregression  $\rho^\tau(\mathbf{s})$  parameters are modelled via spatial Gaussian processes on transformed scales. In particular,  $\sigma^\tau(\mathbf{s})$  captures spatial scale dependence through the Gaussian process  $Z_\sigma^\tau(\mathbf{s}) = \log\{\sigma^\tau(\mathbf{s})\}$ , with mean  $Z_\sigma^\tau$  and exponential covariance function having variance parameter  $\sigma_\sigma^{2,\tau}$  and decay parameter  $\phi_\sigma^\tau$ . In addition,  $\rho^\tau(\mathbf{s})$  captures spatial autoregression dependence through the Gaussian process  $Z_\rho^\tau(\mathbf{s}) = \log\{(1 + \rho^\tau(\mathbf{s}))/(1 - \rho^\tau(\mathbf{s}))\}$ , with mean  $Z_\rho^\tau$  and exponential covariance function having variance parameter  $\sigma_\rho^{2,\tau}$  and decay parameter  $\phi_\rho^\tau$ .

The term  $q_{t\ell}^\tau(\mathbf{s})$  contains fixed and random effects as:

$$q_{t\ell}^\tau(\mathbf{s}) = \beta_0^\tau + \alpha^\tau t + \beta_1^\tau \sin(2\pi\ell/365) + \beta_2^\tau \cos(2\pi\ell/365) + \beta_3^\tau X(\mathbf{s}) + \gamma_t^\tau(\mathbf{s}) \quad (2)$$

Here,  $\beta_0^\tau$  denotes a global intercept,  $\alpha^\tau t$  represents a baseline long-term linear trend in years, the harmonic terms capture the seasonal behaviour, and  $X(\mathbf{s})$  is the standardised altitude at  $\mathbf{s}$ . Remaining spatiotemporal dependence is captured by the random effects  $\gamma_t^\tau(\mathbf{s}) = \beta_0^\tau(\mathbf{s}) + \alpha^\tau(\mathbf{s})t + \psi_t^\tau + \eta_t^\tau(\mathbf{s})$ . In particular,  $\beta_0^\tau(\mathbf{s})$  is a zero-mean Gaussian process with exponential covariance function having variance parameter  $\sigma_{\beta_0}^{2,\tau}$  and decay parameter  $\phi_{\beta_0}^\tau$ , and denotes a local spatial intercept providing location-specific adjustments to the global intercept. Similarly,  $\alpha^\tau(\mathbf{s})$  is a zero-mean Gaussian process with exponential covariance function having variance parameter  $\sigma_\alpha^{2,\tau}$  and decay parameter  $\phi_\alpha^\tau$ , and represents a local spatial long-term trend coefficient. Lastly,  $\psi_t^\tau \sim \text{i.i.d. } N(0, \sigma_\psi^{2,\tau})$  and  $\eta_t^\tau(\mathbf{s}) \sim \text{i.i.d. } N(0, \sigma_\eta^{2,\tau})$  represent global and local annual intercepts, respectively. Both terms are modelled as independent Gaussian random variables and account for year-to-year variability, such as anomalously hot or cold years.

Model inference is conducted within a Bayesian framework (see Section S1 of the Supplementary Materials or Castillo-Mateo et al., 2023, for the full details). Conditionally conjugate prior distributions for all model parameters were specified whenever available to complete the model specification. To perform posterior inference, a Metropolis-within-Gibbs algorithm was employed to obtain MCMC samples from the joint posterior distribution.

As the analysis period spans from May 1st to September 30th,  $\ell = 2, \dots, 153$  (first day is not modelled in the autoregression), while the index for the year  $t = 1, \dots, 15$ , given that we consider 2008 to 2022. We selected  $n_1 = 93$  monitoring sites, denoted by  $S_1$ , that satisfy the condition of having no more than seven consecutive days of missing data. The remaining missing values were imputed using splines, as the AL distribution, although suitable in our case as a working likelihood for consistent quantile estimation (Sriram et al., 2013), does not represent the true data likelihood and should be used carefully to impute the previous day's temperature. The reduction in the number of monitoring stations was due to the high proportion of missing data in the original dataset, as shown in Figure S2 of the Supplementary Materials. A detailed data selection flowchart illustrating this process is provided in the Supplementary Materials (see Figure S3). The locations of the monitoring sites, and their respective altitude, are shown in Figure 1(a).

**Thin plate spline regression** After fitting the GQRM, we plugged the posterior median of the model parameters in Equation 1 to obtain the conditional quantile estimates  $Q_{Y_{t\ell}(\mathbf{s}_i)}^*(\tau \mid Y_{t,\ell-1}(\mathbf{s}_i))$  for each  $\mathbf{s}_i \in S_1$ ,  $t = 1, \dots, 15$ ,  $\ell = 2, \dots, 153$ , and  $\tau \in T$ .

To construct a spatial exposure map for each day, we need the conditional quantile  $Q_{Y_{t\ell}(\mathbf{s}_0)}(\tau \mid Y_{t,\ell-1}(\mathbf{s}_0))$  at arbitrary locations  $\mathbf{s}_0 \in D$ . However, the lagged temperature  $Y_{t,\ell-1}(\mathbf{s}_0)$  is not observed at unmonitored locations. To approximate the exposure surface, we define a spatial grid  $G_1$ , which combines the 378 centroids of municipalities with

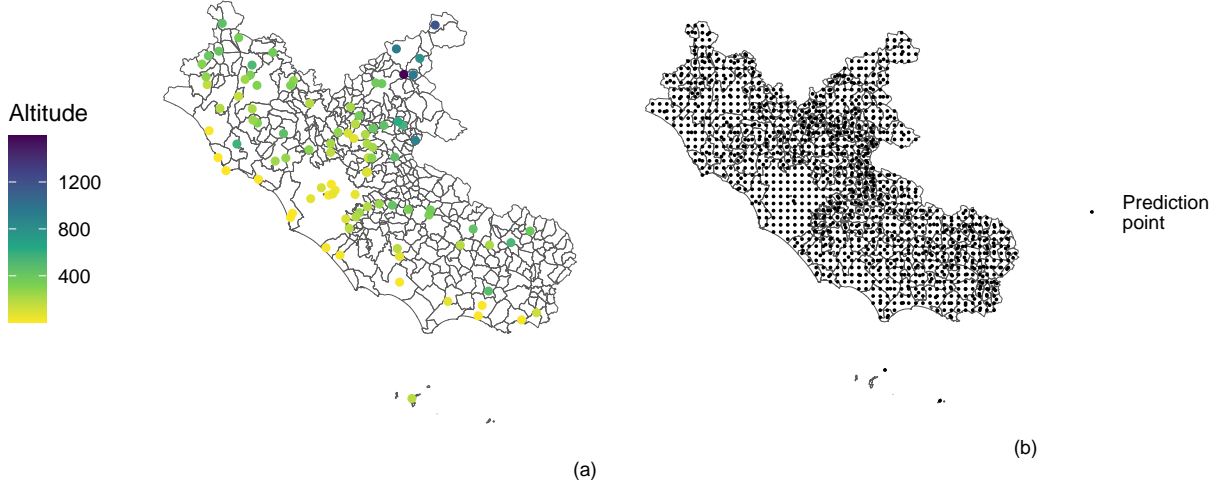


Figure 1: Monitoring stations with altitude information (a), and prediction grid  $G_1$  (b) in the Lazio region.

1000 equally spaced points across the region, resulting in a total of  $|G_1| = 378 + 1000 = 1378$  points that densely and evenly cover the region  $D$ . The locations of the grid are shown in Figure 1(b).

For each year  $t$  and day  $\ell$ , we interpolate the estimated conditional quantiles across space employing a simple thin plate spline (tps) regression (Wood, 2003). Specifically, we fit the model:

$$Q_{Y_{t\ell}(\mathbf{s})}^*(\tau \mid Y_{t,\ell-1}(\mathbf{s})) = f_{t\ell}(\mathbf{s}) + \epsilon_{t\ell}(\mathbf{s}) \quad (3)$$

where  $f_{t\ell}(\cdot)$  is a smooth spatial function estimated by  $\hat{f}_{t\ell}(\cdot)$  minimizing the penalized sum of squares:

$$\sum_{i=1}^{n_1} \left( Q_{Y_{t\ell}(\mathbf{s}_i)}^*(\tau \mid Y_{t,\ell-1}(\mathbf{s}_i)) - \hat{f}_{t\ell}(\mathbf{s}_i) \right)^2 + \lambda J(f_{t\ell}) \quad (4)$$

where  $J(\cdot)$  is a penalty functional measuring the wigginess of  $f_{t\ell}$  and  $\lambda$  controls the trade-off between data fitting and smoothness of  $f_{t\ell}$ . We set  $\lambda = 0.001$  to ensure that the estimated surface closely follows the estimated quantiles.

The interpolated exposure surface across the region is then defined as  $\hat{Q}_{Y_{t\ell}(\mathbf{s}_j)}^*(\tau \mid Y_{t,\ell-1}(\mathbf{s}_j)) = \hat{f}_{t\ell}(\mathbf{s}_j)$  for each  $\mathbf{s}_j \in G_1$ . Municipality-level exposures are finally obtained by averaging the interpolated values across all grid points  $\mathbf{s}_j$  falling within each municipality.

### 2.2.2 Method 2: Geospatial Gaussian process model

The second approach is a Geospatial Gaussian process model (GGPM) that describes the conditional mean of the response variable. Therefore, results can be expected to be comparable to those obtained with the quantile regression at  $\tau = 0.5$ .

Following the notation above, the model can be written as:

$$Y_{t\ell}(\mathbf{s}) = \beta_0 + \beta_1 X(\mathbf{s}) + \xi_{t\ell}(\mathbf{s}) + \epsilon_{t\ell}(\mathbf{s}) \quad (5)$$

In addition to the intercept  $\beta_0$  and the standardised altitude covariate  $X(\mathbf{s})$ , the model includes a measurement error term  $\epsilon_{t\ell}(\mathbf{s}) \sim \text{i.i.d. } N(0, \sigma_\epsilon^2)$ , modelled as a Gaussian white-noise process, and a state process  $\xi_{t\ell}(\mathbf{s})$ , which represents the latent spatiotemporal signal. Specifically, the spatial process  $\xi_{t\ell}(\mathbf{s})$  evolves over time according to a first-order autoregressive process (Harvill, 2010), and is specified as:

$$\xi_{t\ell}(\mathbf{s}) = a \xi_{t,\ell-1}(\mathbf{s}) + \omega_{t\ell}(\mathbf{s}) \quad (6)$$

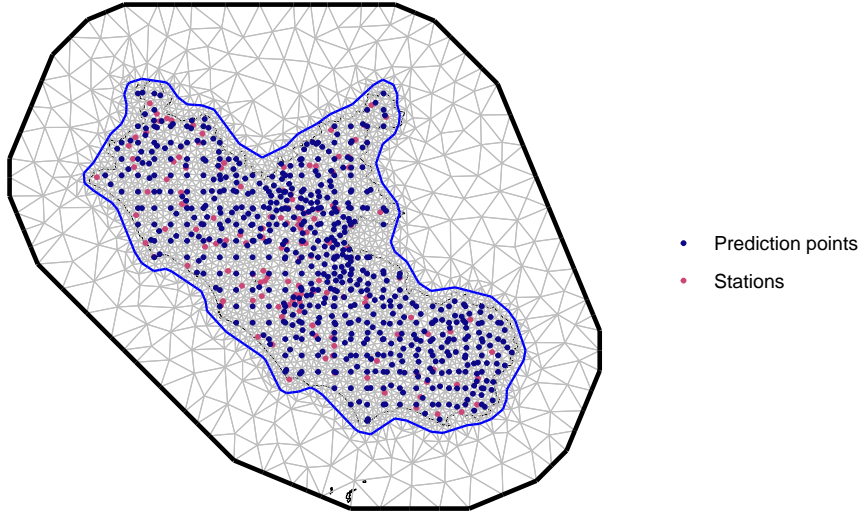


Figure 2: Plot of the mesh in use with the location of the stations  $S_2$  and the prediction points  $G_2$ .

for  $\ell = 2, \dots, 153$  and coefficient  $|a| < 1$ . For  $\ell = 1$ , the process is initialized from its stationary distribution

$$\xi_{t1}(\mathbf{s}) \sim \text{i.i.d. } N\left(0, \frac{\sigma_\xi^2}{1 - a^2}\right) \quad (7)$$

Moreover,  $\omega_{t\ell}(\mathbf{s})$  is a zero-mean Gaussian field, independent in time and, for the same time point, have a variance  $\sigma_\omega^2$  and a correlation function  $\mathcal{C}(h)$ . Here, the correlation function  $\mathcal{C}(h)$  is purely spatial and it is a Matérn function:

$$\mathcal{C}(h) = \frac{1}{\Gamma(\nu)2^{\nu-1}}(kh)^\nu K_\nu(kh) \quad (8)$$

where  $h = \|\mathbf{s} - \mathbf{s}'\|$  is the absolute Euclidean distance between two spatial points  $\mathbf{s}, \mathbf{s}' \in D$ ,  $K_\nu$  denoting the modified Bessel function of the second kind and order  $\nu > 0$ . The parameter  $\nu$  measures the degree of smoothness of the process, and the scaling parameter  $k > 0$  controls the spatial correlation range.

The model is implemented within the R-INLA package (Rue et al., 2009; Martins et al., 2013; Van Niekerk et al., 2023), using the SPDE approach (Lindgren et al., 2011; Blangiardo et al., 2013; Cameletti et al., 2013; Riley et al., 2025) to represent a continuous spatial process as a discretely indexed spatial random process. This produces substantial computational advantages since it avoids the so-called *big n problem* that affects spatial Gaussian processes (Jona Lasinio et al., 2013). As shown in Lindgren et al. (2011), within the SPDE approach the spatial correlation structure is modelled by solving the linear fractional SPDE:

$$(k^2 - \Delta)^{\alpha/2}(\tau u(\mathbf{s})) = W(\mathbf{s}) \quad (9)$$

with  $k > 0$  spatial scale parameter,  $\alpha$  governs the smoothness of the field,  $\Delta$  is the Laplacian operator, and  $W(\mathbf{s})$  is Gaussian white noise. This yields a Matérn covariance function with smoothness  $\nu = \alpha - d/2$ , where  $d$  is the spatial dimension (here  $d = 2$ ). The approximation employs a linear combination of basis functions, defined in a triangulated domain called a mesh. In our application, to discretize the spatial domain, we construct a non-convex mesh using a resolution adapted to the density of prediction and observation points. We constructed the mesh shown in Figure 2, with a fine maximum edge length of 4.5 km and 20 km, for the inner and outer meshes, respectively, and the boundaries determined by the full grid coordinates.

To fit the model, we selected  $n_2 = 140$  monitoring sites, denoted by  $S_2$ , under the constraint that each site has less than 20% missing observations (see Supplementary Figure S2). This approach leverages the ability of the Bayesian approach to handle missing data through model-based imputation. Due to computational limitations, we estimated a separate model for each year  $t = 1, \dots, 15$ , treating them independently. Given the observed values of  $Y_{t\ell}(\mathbf{s})$ , we rely on the

posterior predictive distribution to obtain realisations  $Y_{t\ell}(\mathbf{s}_j)$ , for each grid point  $\mathbf{s}_j \in G_2$ , built as before but with 250 equally spaced points for a total of  $|G_2| = 628$  due to computationally restraints,  $\ell = 1, \dots, 153$  and  $t = 1, \dots, 15$ . In the prediction stage, each location  $\mathbf{s}_j \in G_2$  was assigned the average altitude of the municipality in which it is located. The Bayesian approach, through the INLA algorithm, provides the posterior distribution of  $\xi$  for all the  $n_2 + |G_2|$  triangulation vertices, so it is straightforward and computationally convenient to obtain predictions for  $Y_{t\ell}(\mathbf{s}_j)$  as:

$$f(Y_{t\ell}(\mathbf{s}_j) | \mathbf{y}) = \int f(Y_{t\ell}(\mathbf{s}_j) | \boldsymbol{\theta}) f(\boldsymbol{\theta} | \mathbf{y}) d\boldsymbol{\theta} \quad (10)$$

where  $\boldsymbol{\theta}$  is the set of model parameters and  $\mathbf{y}$  are the observed data. Lastly, as in the previous method, we can compute municipality-level temperatures as average of all  $\mathbf{s}_j$  locations falling within each municipality.

### 2.2.3 Method 3: ERA5-Land data

As a benchmark, we consider the method commonly used in the literature, which is based on hourly air temperatures extracted from the ERA5-Land dataset (Muñoz-Sabater et al., 2021). We first computed for each day the maximum temperature and then obtained municipality-level values using area-weighted averages. Given  $\{C_1, \dots, C_K\}$ , the ERA5-Land grids that fall within the Lazio region, the temperature for the municipality  $m_i$  on day  $\ell$  and year  $t$  is given by:

$$Y_{t\ell}(m_i) = \frac{1}{A_{m_i}} \sum_{k=1}^K A_{m_i k} Y_{t\ell}(C_k) \quad (11)$$

where  $A_{m_i}$  is the total surface of the municipality  $m_i$ , for  $i = 1, \dots, 378$ , and  $A_{m_i k}$  is the surface of the cell  $C_k$  that falls in the municipality  $m_i$ . The total surface of the municipality can also be expressed as  $A_{m_i} = \sum_{k=1}^K A_{m_i k}$ , this is the sum of the proportion of the grid cells within its borders.

## 2.3 Stage 2: Epidemiological modelling

In the second stage of the analysis, we assessed the association between exposure to high temperatures and mortality due to cardiovascular and respiratory causes. To this end, we used the temperature estimates obtained from the three spatiotemporal methods described in the previous section as exposure in the following epidemiological models.

We adopted a time-stratified case-crossover design, commonly used for analysing the effect of transient exposures (Lu and Zeger, 2007; Navidi and Weinhandl, 2002). The temperature on the day of the cardiovascular/respiratory death (event day) is compared with the temperature on non-event days. Within this design, each case acts as its own control, intrinsically adjusting for individual-level factors that do not vary over time (e.g. age, sex, ethnicity, deprivation). We selected non-event days as the same day of the week, calendar month and year as the event day to avoid overlap bias (Konstantinoudis et al., 2022, 2023). Following Michelozzi et al. (2004, 2009) and Singh et al. (2024), each individual case was linked to the average daily maximum temperature in the 3 days before the event day and the corresponding control days.

In order to simplify notation, differently from the spatiotemporal exposure models in Section 2.2, here we use  $t$  to denote days between June and August in the years 2008 to 2022.

Let  $O_{tj}$  be the case-control identifier at time  $t$  and in the  $j$ -th case-control group. Then  $X_{tjh}$  is the exposure for the  $j$ -th case-control group, defined as the mean daily maximum temperature estimated by the  $h$ -th method ( $h = 1, 2, 3$  as in Section 2.2), in the 3 days prior to the event (or control) day  $t$ . Finally,  $\text{holiday}_t$  is a binary variable 1/0 indicating if the  $t$ -th day is a bank holiday. We specified Bayesian hierarchical conditional Poisson models as:

$$\begin{aligned} O_{tj} &\sim \text{Poisson}(\mu_{tj}) \\ \log(\mu_{tj}) &= \beta_0 + f_{rw2}(X_{tjh}) + \beta_1 \cdot \text{holiday}_t + u_j \\ X_{tjh} | X_{(t-1)jh}, X_{(t-2)jh}, \tau_X &\sim N(2X_{(t-1)jh} - X_{(t-2)jh}, \tau_X^{-1}) \\ \tau_X &\sim \text{PCprior} \left( P \left( \tau_X^{-1/2} > 0.1 \right) = 0.01 \right) \\ u_j &\sim N(0, 100) \\ \beta_0, \beta_1 &\sim N(0, 1000) \end{aligned} \quad (12)$$

where  $\beta_0$  and  $\beta_1$  are the coefficients associated with the intercept and the holiday variable, respectively;  $f_{rw2}(\cdot)$  is a second-order random walk, used to model the temperature effect; and  $u_j$  is a fixed effect corresponding to the event/non-event day grouping. We adopted weakly informative priors for the regression coefficients and the group effect, while a penalised complexity prior was specified for the second-order random walk smoothing term to ensure interpretable regularisation and to avoid excessive flexibility unsupported by the data.

### 2.3.1 Heatwaves

The definition of a heatwave is not straightforward, as it involves both a temperature metric, a temperature threshold, and the duration of consecutive days exceeding that threshold. In the analyses, we considered four different thresholds and three duration criteria (Xu et al., 2016; Guo et al., 2017; Kang et al., 2020) for daily maximum temperatures. For the threshold we evaluated three empirical quantiles (0.90, 0.925, 0.95) of the daily maximum temperature time series in the summer for each municipality, as well as a fixed value at 35°C (Vecellio et al., 2022; Vanos et al., 2023). For the duration we considered: (a) surpassing the threshold, which is labelled as *heatwave\_base*; (b) being exposed to at least 2 consecutive days above the threshold; (c) being exposed to at least 3 consecutive days above the threshold. For (b) and (c) we also excluded the first day that the temperature surpasses the threshold as a heatwave day, to better capture the prolonged effect of sustained heat (Rocklov et al., 2012). These two scenarios are labelled as *heatwave\_1daylag* and *heatwave\_2dayslag*, respectively. Similarly to the temperature lag, a subject is considered affected by a heatwave if a heatwave day occurs in their municipality on the day of the event or during any of the three preceding days.

We estimated models including the heatwave variable, using the same specification as in Equation 12, with the addition of a binary covariate  $heatwave_{tjhz}$ . The variable indicate whether, in the three days preceding the event day  $t$ , the  $j$ -th group was exposed to at least one heatwave day, defined according to the  $h$ -th spatiotemporal model and the  $z$ -th combination of temperature threshold and heatwave definition. The corresponding regression coefficient,  $\beta_2$ , was assigned a prior distribution  $\beta_2 \sim N(0, 1000)$ , consistent with the other fixed effects.

## 2.4 Implementation

All analyses were conducted using R (version 4.4.2, R Core Team, 2024). The GQRM was fitted using the MCMC algorithm described in Castillo-Mateo et al. (2023), while tps's were estimated using the `fields` package (Douglas Nychka et al., 2021). GGPM and epidemiological models were implemented with R-INLA (Lindgren and Rue, 2015). Municipality-level area weighted averages from the ERA5-Land data were computed using the `extract` function of the `terra` package (Hijmans, 2024).

## 3 Results

### 3.1 Spatiotemporal models

In the following, we compare the temperatures obtained using the three different methods presented in Section 2.2. For method 1, GQRM, we show results on the median ( $\tau = 0.5$ ) in order to allow comparison with the other two approaches.

Prior to presenting the modelling results, Figure S4 in the Supplementary Materials shows a quantile–quantile (QQ) plot comparing daily maximum temperatures from ground monitoring stations with the nearest ERA5-Land reanalysis grid cell within the study region. The plot indicates that while ERA5-Land tends to slightly overestimate lower temperature values, it systematically underestimates those in the upper range.

Figure 3 displays the temporal trend of estimated daily maximum temperatures produced by the three spatiotemporal methods. The difference between the station-based approaches and the Copernicus ERA5-Land reanalysis is immediately evident, particularly in the warmest provinces of the region, Frosinone and Latina. An overall increasing trend in temperature over the years is also observed.

Yearly estimates between the three methods are shown in Table S1 of the Supplementary Materials, and it is possible to notice the growing overall trend and how the differences between the methods vary slightly over the years.

An example of the spatial differences between the three methods is shown in Figure 4. All models capture the main spatial patterns: the northern part of the region is consistently colder, while the area just north of Rome appears to be the the warmest. In the ERA5-based method, coastal municipalities exhibit a more temperate climate compared to inland areas (Muñoz-Sabater et al., 2021), a feature not observed in the station-based methods. The GGPM approach displays the greatest variability between neighbouring municipalities, possibly due to the inclusion of altitude as a covariate in the model predictions. All daily and monthly maps comparing the methods are available through an interactive Shiny App.<sup>1</sup>

<sup>1</sup>[https://emilianoceccarelli.shinyapps.io/temperature\\_comparison\\_Lazio/](https://emilianoceccarelli.shinyapps.io/temperature_comparison_Lazio/)

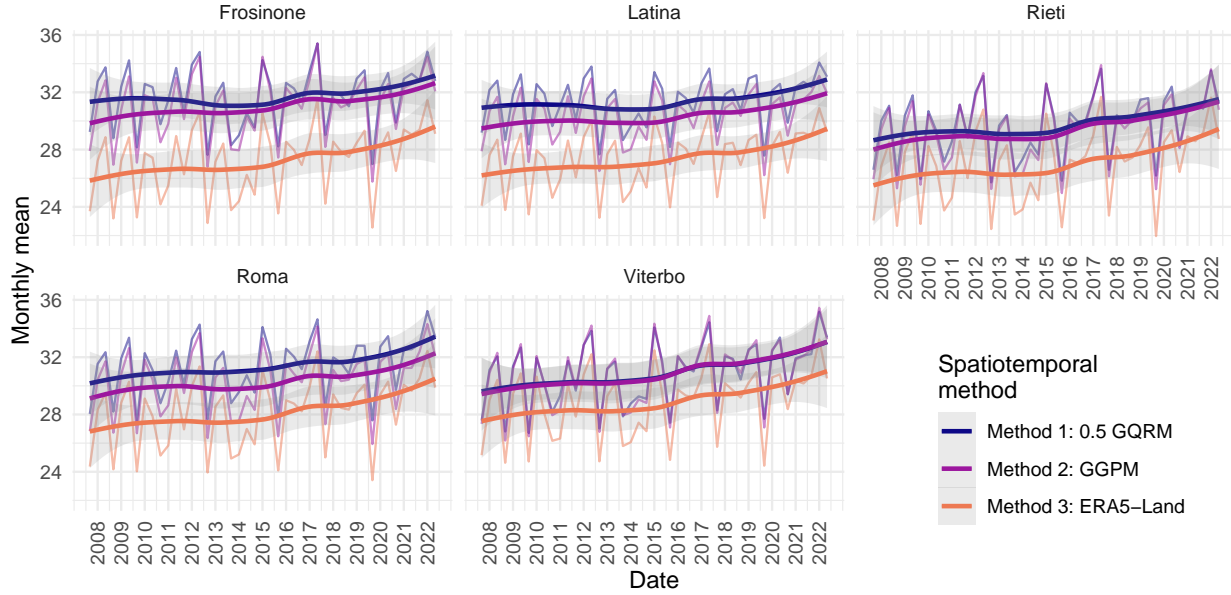


Figure 3: Averages of daily maximum temperatures ( $^{\circ}\text{C}$ ) in the summer months, estimated by the three methods across the five provinces of Lazio. The general trend is drawn using LOESS regression with a 95% confidence interval.

### 3.2 Epidemiological models

We included 83,381 death events in the study, and a more detailed study profile is reported in Figure 5. Of the total, 45% were males and 55% females. The average age at death was 83 years (interquartile range: 79–91). The spatial distribution was uneven, with 71% of deaths occurring in the province of Rome, reflecting the underlying population density. After creating the control cases, each model was fitted on a total of 369,901 observations (83,381 cases and 286,520 controls).

Figure 6 shows the relationship between temperature and mortality, expressed in terms of relative risk (RR). We fitted the models described in Equation 12, applying temperature exposures derived from the three different spatiotemporal methods. As in the previous section, the figure presents results for the 0.5 GQRM only to facilitate comparison with the other two approaches. Detailed plots for all GQRM considered in the analysis are available in the Supplementary Materials (see Figure S5). Each curve has been normalised so that  $RR = 1$  at the temperature corresponding to the lowest mortality risk. This temperature is often referred to as the optimal temperature or minimum mortality temperature (MMT) (Gasparrini et al., 2015; Lopez-Bueno et al., 2021), facilitating interpretation and comparison across exposure surfaces. In line with previous literature (Armstrong, 2006; Gasparrini et al., 2015), the estimated RR curves exhibit a J-shaped relationship, with steeper increases in risk at high temperatures. All spatiotemporal methods capture the elevated risk associated with extreme heat, but differ in the MMT. As shown in Table 1, the MMT varies by up to  $2^{\circ}\text{C}$  when comparing the ERA5-Land-based estimates to the GGPM, and by more than  $3^{\circ}\text{C}$  compared to the median GQRM. Table S2 in the Supplementary Materials reports the MMTs for all quantile levels, showing that the 0.05 GQRM returns an MMT closest to the ERA5-Land estimate.

Estimates for the *holiday* coefficient are in agreement between models and indicate a  $-11.27\%$  reduction in mortality risk compared to non-holiday days (95% credible interval:  $-15.66\%$  to  $-6.65\%$ ).

We performed stratified analyses by age class (18–64, 65–79, 80+, and 18+) and sex. Figure 7 shows the RR curves for the sex specific curves across all ages and for the most vulnerable age group (80+). Females show a more consistent increase in risk beginning at lower temperatures, and leading to slightly higher RRs compared to males. Additionally, the 80+ group also exhibits a pronounced increase of RR at lower temperatures compared to the total population, indicating high vulnerability to extreme heat.

The complete results are shown in Figure S6 of the Supplementary Materials and overall they are consistent across spatiotemporal temperature methods. No apparent increase in risk is observed for the 18–64 age group, while a general

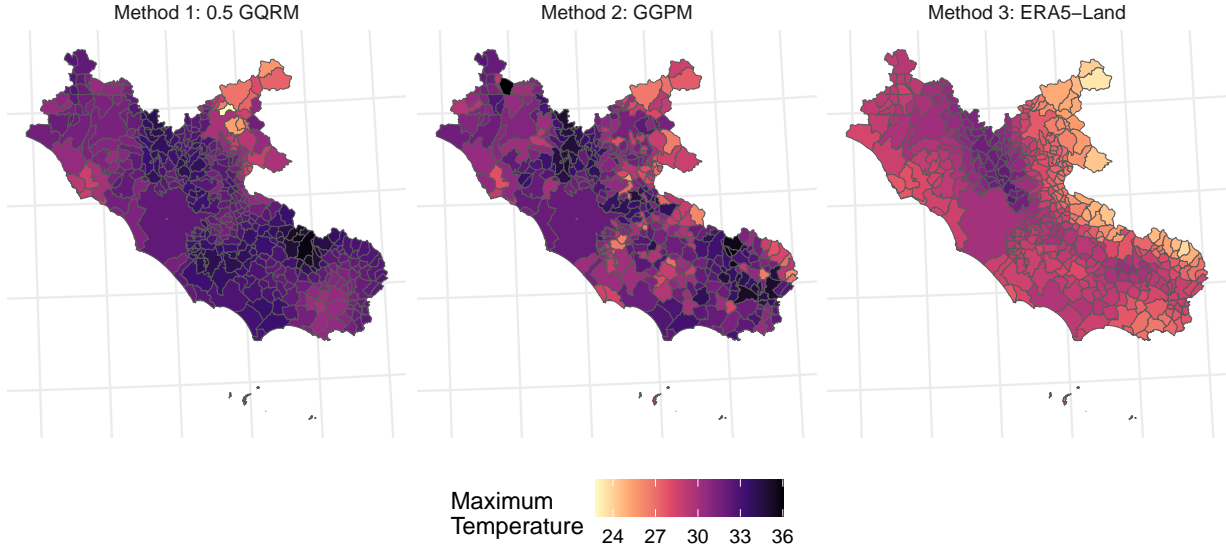


Figure 4: Average daily maximum temperature (°C) per municipality and spatiotemporal methods in July 2022.

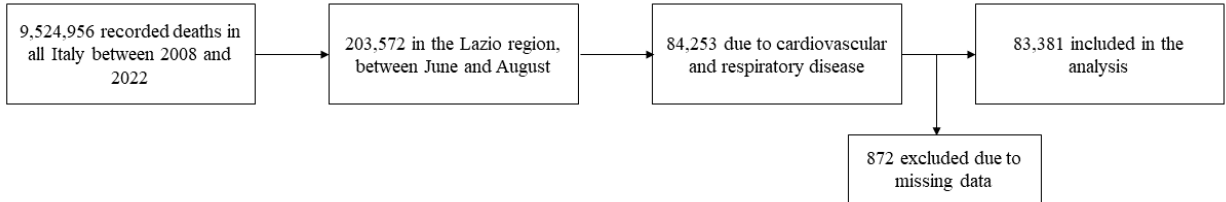


Figure 5: Study profile.

upward trend is visible for the 65–79 group, especially among females, although there is no strong evidence of a clear difference.

### 3.2.1 Heatwaves assessments and model

Each spatiotemporal method and each heatwave definition (as described in Section 2.3.1) results in a different number of days being formally classified as heatwaves. As shown in Figure S7 of the Supplementary Materials, the differences across temperature datasets are not substantial as long as the threshold is defined based on the municipality-specific time series.

Figure 8 presents the average number of days that a municipality in the region has experienced per duration criteria, spatiotemporal temperature method and temperature threshold. The plots highlight the increasing trend in heatwave occurrence over time and shows how the use of a fixed temperature threshold is sensitive to the underlying temperature source. Despite methodological differences, all spatiotemporal models and quantile thresholds consistently capture the temporal dynamics of heatwaves over the study period.

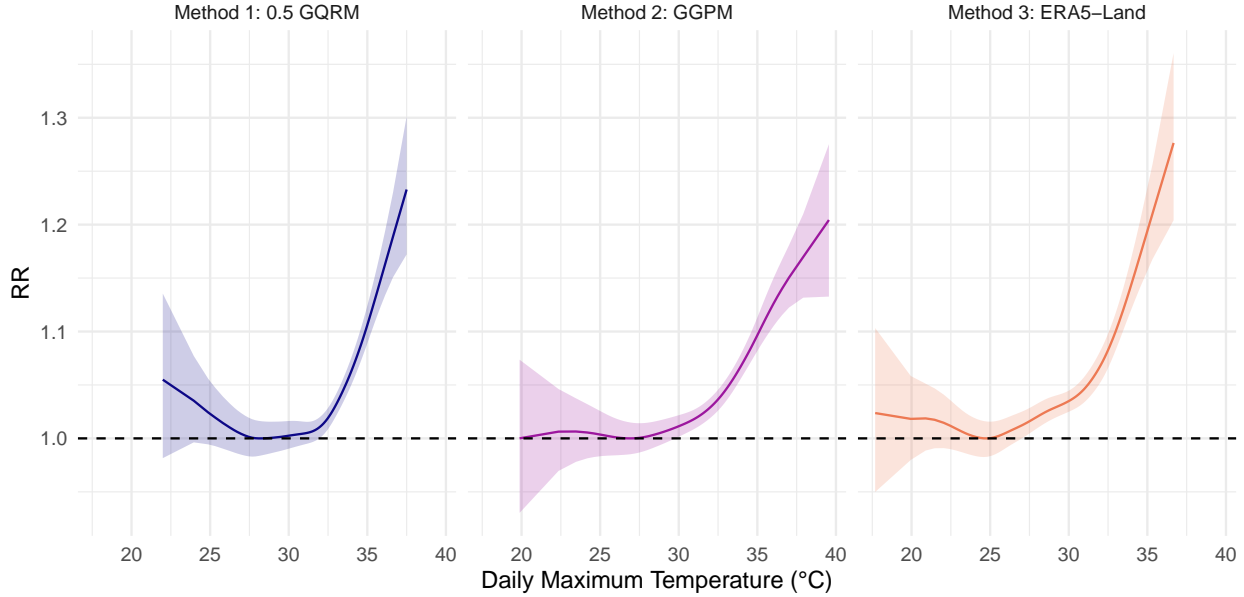


Figure 6: RR estimates for daily maximum temperature exposure by spatiotemporal methods. Shaded area indicates 95% credible interval.

Figure 9 shows the estimated RRs associated with the heatwave variable in the model presented in Section 2.3.1, along with their corresponding 95% credible intervals. Estimates based on the fixed 35°C threshold are quite variable and generally pushed towards 0. This is likely due to multicollinearity with the continuous temperature variable. To support this claim, we estimated again the models without the continuous temperature variable. The results, reported in Figure S8 of the Supplementary Materials, show that the estimated RRs remain consistently above 1 and comparable across spatiotemporal models, duration criteria, and thresholds, even when using the fixed 35°C threshold. Considering the 90th percentile threshold, the relative risks are around 1.02 for the 0.5 GQRM using the three heatwave definitions, while stronger effects are seen for the GGPM and ERA5-Land temperature model, particularly in combination with stricter heatwave duration criteria. As the quantile threshold increases, RR estimates tend to stabilize across spatiotemporal methods; an exception is the 95% quantile for the two days lag criterion, where the RR estimates are characterised by large uncertainties, suggesting a potential trade-off between threshold severity and statistical power. The temperature-mortality RR curve retains its overall shape even when the heatwave variable is included, as shown in Figure S9 of the Supplementary Materials. When comparing these curves with those estimated from the previous model (see Figure 6), a slight decline is seen in the curves for high temperatures when a balanced heatwave definition is applied, that is, a combination of threshold and duration criteria that captures sustained heat exposure without being overly restrictive. This suggests that part of the effect attributed to high temperatures may be explained by discrete heatwave events.

### 3.3 Sensitivity analysis

As a sensitivity analysis, we estimated models 12 selecting malignant neoplasm (ICD-10 codes C00–C97) as the underlying cause of death. This outcome was chosen as a negative control because, unlike cardiovascular and respiratory diseases, cancer mortality is not expected to be acutely affected by short-term fluctuations of daily maximum temperature. Additionally, the large number of malignant neoplasm mortality (58,917 cases and 202,086 controls) ensured a sample size comparable to that of cardiovascular and respiratory causes considered in the main analyses.

Consistent with our expectations, there was not evidence of an association between high temperatures and mortality, with effect size close to 0 across all spatiotemporal temperature exposure estimation methods. RR estimates are shown in Figure S10 of the Supplementary Materials.

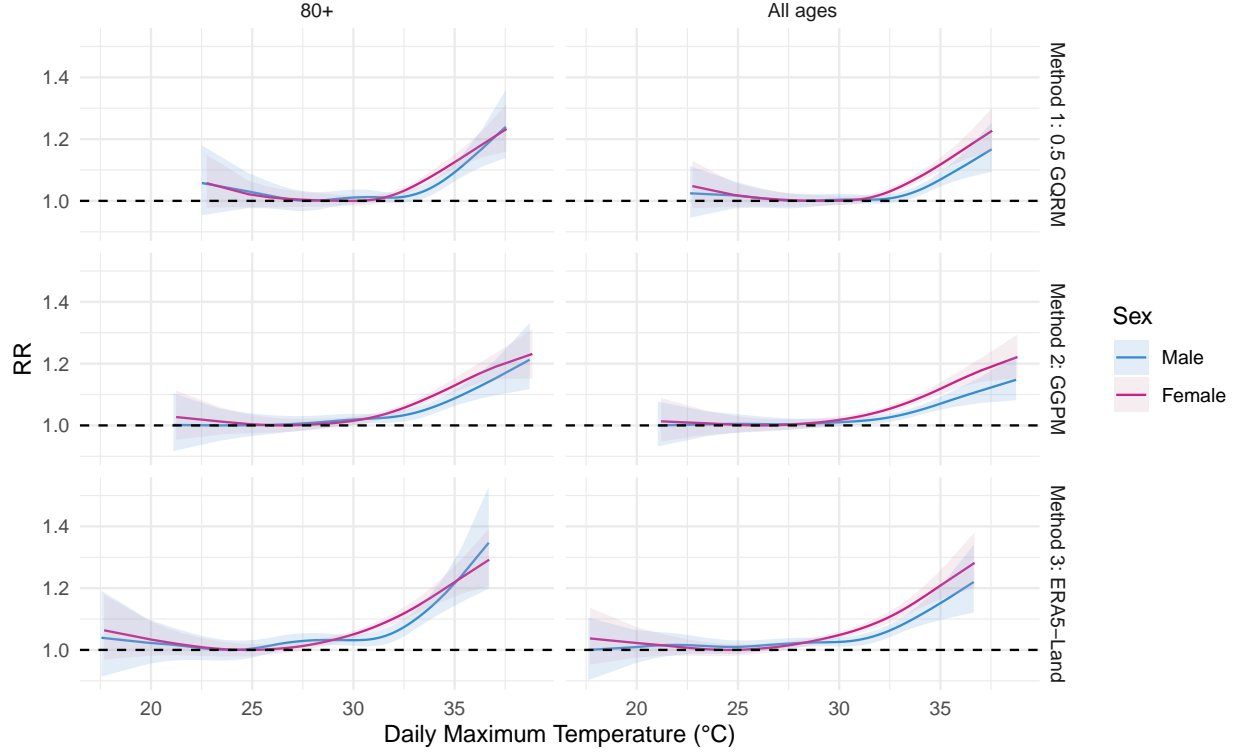


Figure 7: RR estimates for maximum temperature exposure by spatiotemporal method, age group (80+ and total population), and sex. Shaded areas indicates 95% credible intervals.

#### 4 Discussion and conclusions

Using established methods, we compared three approaches for deriving municipality-level exposure surfaces to extreme heat. In the first stage, we estimated daily maximum temperatures using two model-based spatiotemporal methods relying on weather station data, and one GCD reanalysis, Copernicus' ERA5-Land. Our results show spatial variability across the three approaches. ERA5-Land GCD systematically produced lower temperatures in coastal municipalities compared to inland areas, an effect not observed in the station-based approaches. This discrepancy can be explained by the averaging process over mixed land-sea grid cells, which reduces estimates for municipalities bordering the coastline. A similar effect was observed in mountainous regions, where valley settlements may inherit cooler estimates due to the influence of neighbouring high-altitude grid cells. These findings are consistent with previous literature reporting limitations of ERA5-Land in complex terrains, as shown by Mistry et al. (2022), who noted that the ERA5-Land reanalysis might perform worse in tropical regions. The two station-based modelling approaches produced consistently higher temperatures than the satellite-based estimates. Among them, the GQRM combined with thin based splines (Method 1) yielded the highest values. The tps interpolation used in this method provided smoother spatial patterns, whereas the GGPM (Method 2) captured sharper variability between neighbouring municipalities, reflecting the inclusion of altitude as a covariate. We might consider a calibration or data fusion approach in a Bayesian modelling framework. However, in this study, our focus is on detecting the effects of high temperatures; therefore, merging station observations with ERA5-Land estimates could mask potential evidence in this regard.

The three methods were compared in an epidemiological context, assessing the relationship between heat exposure and mortality from cardiovascular and respiratory diseases. In accordance with existing literature, our models found that despite using different temperature sources and methods, the exposure-response J-shaped curve remains largely unchanged. Royé et al. (2020) noted that the mortality risk estimates using ERA5-Land were slightly lower than those using measuring stations. This differs from our estimates, as we find a slightly higher RR using the temperatures derived by ERA5-Land, as shown in Figure 6. The interpretation of the maximum RR must be considered relative to the MMT, which is lower for ERA5-Land, as reported in Table 1, and thus shifts the point of reference for comparison. A similar result is found by Choi and Bell (2023), who found more than 3°C of difference in MMTs between station-based

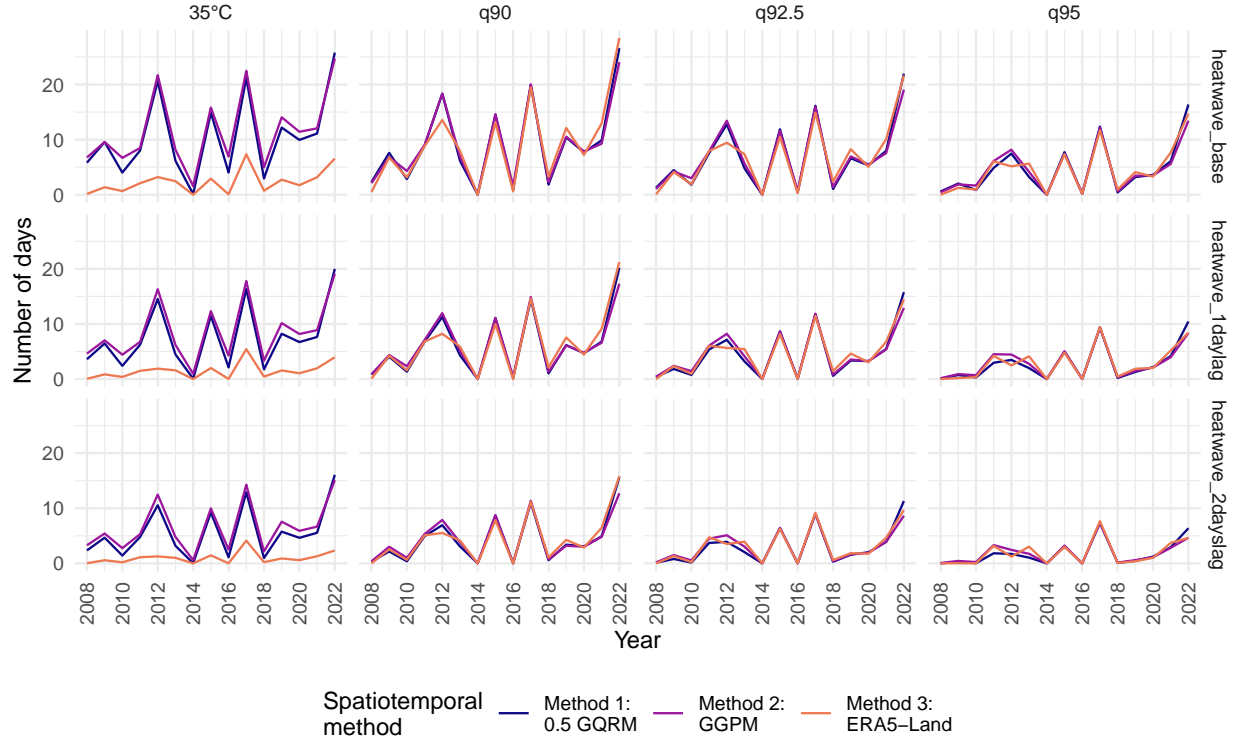


Figure 8: Average annual number of heatwave days per duration criteria, spatiotemporal temperature method and temperature threshold.

models and a GCD. Overall, the three approaches provide broadly consistent estimates, reinforcing the robustness of the observed association.

From a public health perspective, the differences observed in the estimated MMTs open a discussion for the design of early warning systems. The wide spatial coverage of ERA5-Land ensures that every municipality can be assigned an exposure value, making it a valuable tool for regional or national surveillance systems. However, its tendency to underestimate temperatures in complex terrains may potentially trigger warnings in advance. Conversely, monitoring stations provide highly accurate observations, but their sparse and uneven distribution limits their applicability, unless coupled with a modelling approach which allows municipality-specific estimates.

In the Lazio region, the current heat warning system is coordinated by the regional Department of Epidemiology and it is based on four alert levels, with level 3 activated when three consecutive days are forecasted to exceed a municipality-specific threshold of maximum temperature (Dipartimento di Epidemiologia, Regione Lazio, 2025). In this context, differences in MMT estimation across exposure models and temperature sources may directly influence the identification of critical days and the timing of interventions.

Given that early warning systems are inherently based on both intensity and persistence of extreme heat, we further examined the role of heatwaves as prolonged exposure events. Adding the heatwave specification in the models allowed us to investigate whether prolonged exposure to extreme heat conveys an additional risk, beyond that captured by continuous temperature variable. Consistent with previous work (Gasparrini and Armstrong, 2011), we found that including a categorical heatwave indicator did not substantially alter the overall exposure-response curve. However, contrary to Guo et al. (2017), who modelled exposure using daily mean temperatures, our results based on daily maximum temperatures showed strong evidence of an for the heatwave variable after controlling for daily temperature. This suggests that, with an appropriate heatwave definition, epidemiological models can provide further insight into the health risks of prolonged exposure to extreme heat.

When stratifying the analysis by age groups and sex, we found variability in the dose-response curves, particularly for younger ages. As the majority of deaths is observed in the 80+, as expected the dose-response was similar to the all ages one. In both cases, the curves for females tend to rise earlier and remain consistently above those for males.

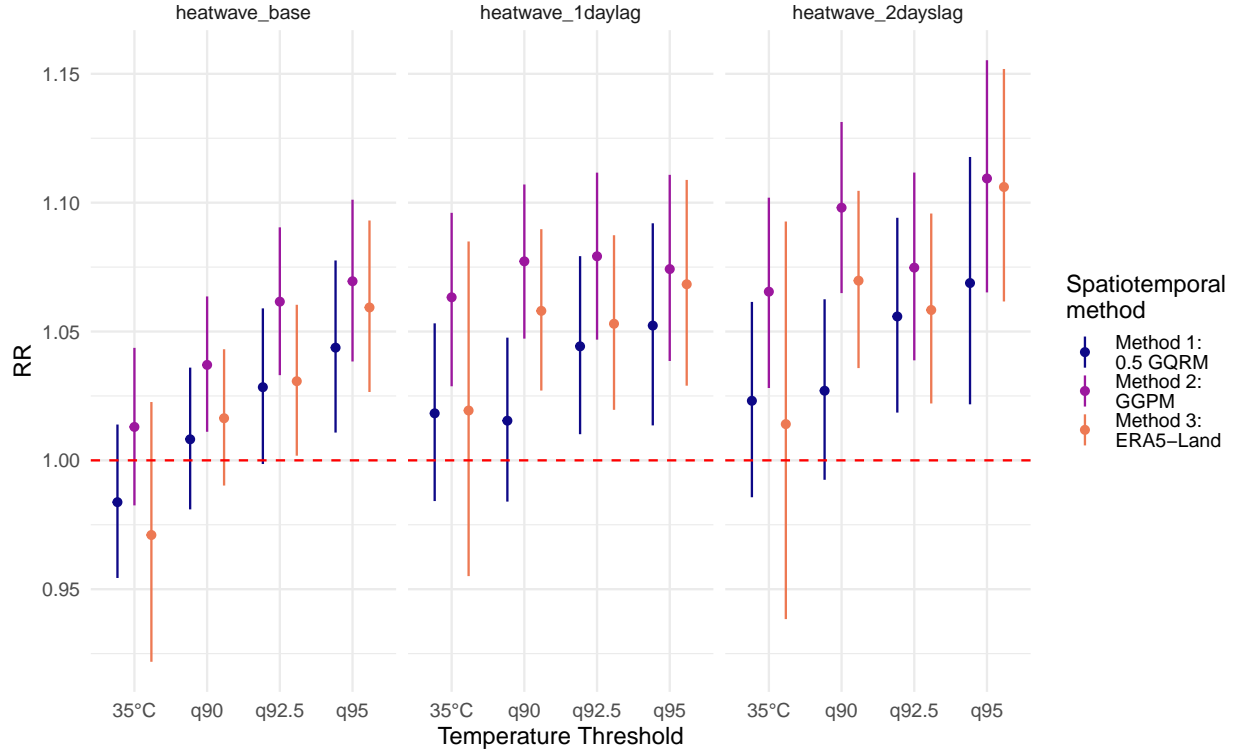


Figure 9: RR estimates and their 95% credible interval of the heatwave variable in the model presented in Section 3.2.1. Results per duration criteria, spatiotemporal temperature method and temperature threshold.

This indicates that females (and specifically older ones) become at increased risk of heat-related mortality at lower temperatures than their male counterparts. This gendered vulnerability is consistent with the literature on the topic (Van Steen et al., 2019), but the underlying reasons for this are not well understood. Enhanced vulnerability to heat can be explained by a higher prevalence of multi-morbidity in women compared to men, partially because females have a higher life expectancy compared to males (Abad-Díez et al., 2014). Many chronic diseases of ageing are exacerbated by high temperatures, or affect thermoregulation directly. For instance, glycaemic regulation is impaired by heat in diabetic patients, but so are other homeostatic activities like sweating Kenny et al. (2016) impairing their ability to dissipate heat. Furthermore, multi-morbidity leads to the use of multiple medications. A recent meta-analysis by Hespers et al. (2024) identified multiple treatments for ageing-related diseases amongst the ones impairing temperature regulation during heat stress. Although females have been observed to have an inherently impaired ability to thermoregulate, these differences are negligible once body size and surface area have been accounted for (Kaciuba-Uscilko and Grucza, 2001). On the contrary, it appears that heat illness is much more prevalent in males than in females, (Gifford et al., 2019) which might explain the small increase in heat-related mortality rates in the males youngest age group, despite not being characterised by strong evidence of an effect.

Thanks to the availability of individual data, we adopted a case-crossover methodology that offers important advantages in environmental epidemiology. By comparing each subject to themselves at different times, it provides strong control for all individual characteristics that do not vary over time, reducing the risk of confounding (Janes et al., 2005).

Whilst the spatiotemporal approaches allowed us to construct precise exposure profiles within the cities, we were forced to match the aggregation of health data, aligning at the municipality scale. In Lazio, this issue mainly concerns the city of Rome, the only municipality with a large enough territorial extension to encompass substantial intra-urban temperature variability.

Several extensions to this work are possible. The framework presented can be generalised to different study regions and health outcomes. Extending the analysis to the national scale will require a different spatiotemporal modelling strategy, as the larger spatial domain and high number of monitoring stations may challenge current specifications. A different

development will be the propagation of posterior uncertainty from the Bayesian exposure models into the second-stage epidemiological estimation, allowing for coherent joint inference across the two stages of the analysis.

### Acknowledgments

E.C. was supported by the European Union – NextGenerationEU, under the PNRR project “C\_PA - DM118 P.A. Pubblica Amministrazione: Metodologie statistiche per il supporto alle decisioni in contesto sanitario pubblico: stima dell’impatto degli eventi climatici estremi sulla salute della popolazione generale e la costruzione di modelli di allerta rapida”, CUP: B53C23002660006, Missione 4, Componente 1 (Missione I.4.1, PNRR Scholarships for Public Administration).

E.C. and G.J.L. were partially supported by the Sapienza University project “Leaving No One Behind: Methods for Sustainability” ID nr.: RD124190DA1146AA - CUP: B83C24007080005.

J.C.-M. was partially supported by MCIU (PEICTI 2024) under Mobility Grant CAS24/00229 (research visit at Sapienza University of Rome); MCIU/AEI/10.13039/501100011033/FEDER,UE under Grant PID2023-150234NB-I00; and Gobierno de Aragón under Research Group E46\_23R: Modelos Estocásticos.

S.G. was supported by the Doctoral Training Programme “Science and Solutions for a Changing Planet” Scholarship (SSCP-DTP) provided by the Natural Environment Research Council (NERC) via the Grantham Institute for Climate Change and the Environment, Imperial College London.

M.B. was partially supported by the MRC Centre for Environment and Health, (Grant number: MR/L01341X/1) and the NIHR Health Protection Unit in Chemical and Radiation Threats and Hazards.

### Data and code availability

Ground monitoring station data are available at <https://scia.isprambiente.it/dati-e-indicatori/>. ERA5-Land data can be obtained from the Copernicus Climate Data Store at <https://cds.climate.copernicus.eu/datasets/reanalysis-era5-land?tab=overview>. Municipal elevation data are provided by ISTAT at <https://www.istat.it/classificazione/principali-statistiche-geografiche-sui-comuni/>. Mortality data are available from Istituto Superiore di Sanità but restrictions apply to the availability of these data, which were used under license for the current study, and so are not publicly available. Data are, however, available from the authors upon reasonable request and with permission of Istituto Superiore di Sanità. Requests for access to the mortality dataset should be directed at: [giada.minelli@iss.it](mailto:giada.minelli@iss.it). The code to replicate the analyses is available on GitHub at [https://github.com/emilianoceccarelli/temperatures\\_mortality](https://github.com/emilianoceccarelli/temperatures_mortality).

### Author contributions

E.C., J.C.-M. and M.B conceived the study. E.C. prepared the data and performed the analyses. M.B., G.M. and G.J.L. contributed to the interpretation of the results. E.C. and S.G. drafted the manuscript. M.B., J.C.-M. and G.J.L. revised the manuscript and all authors approved the final version.

### Conflict of interest

The authors declare no potential conflict of interests.

### Supporting information

The following supporting information is available as part of the online article:

### References

José María Abad-Díez, Amaia Calderón-Larrañaga, Antonio Poncel-Falcó, Beatriz Poblador-Plou, José Manuel Calderón-Meza, Antoni Sicras-Mainar, Mercedes Clerencia-Sierra, and Alexandra Prados-Torres. Age and gender differences in the prevalence and patterns of multimorbidity in the older population. *BMC geriatrics*, 14(1):75, 2014.

Rossella Alfano, Francesca De’Donato, Paolo Vineis, and Marina Romanello. Lancet countdown indicators for Italy: tracking progress on climate change and health. *Epidemiologia e Prevenzione*, 2023.

Ben Armstrong. Models for the relationship between ambient temperature and daily mortality. *Epidemiology*, 17(6): 624–631, 2006.

Benedict G Armstrong, Zaid Chalabi, Bridget Fenn, Shakoor Hajat, Sari Kovats, Ai Milojevic, and Paul Wilkinson. Association of mortality with high temperatures in a temperate climate: England and Wales. *Journal of Epidemiology & Community Health*, 65(4):340–345, 2011.

Michela Vaccini, Annibale Biggeri, Gabriele Accetta, Tom Kosatsky, Klea Katsouyanni, Antonis Analitis, H Ross Anderson, Luigi Bisanti, Daniela D’Ippoliti, Jana Danova, et al. Heat effects on mortality in 15 European cities. *Epidemiology*, 19(5):711–719, 2008.

Joan Ballester, Marcos Quijal-Zamorano, Raúl Fernando Méndez Turrubiates, Ferran Pegenaute, François R Herrmann, Jean Marie Robine, Xavier Basagaña, Kathryn Tonne, Josep M Antó, and Hicham Achebak. Heat-related mortality in Europe during the summer of 2022. *Nature medicine*, 29(7):1857–1866, 2023.

Adrian Gerard Barnett. Temperature and cardiovascular deaths in the US elderly: changes over time. *Epidemiology*, 18(3):369–372, 2007.

Raquel Benavides, Fernando Montes, Agustín Rubio, and Koldo Osoro. Geostatistical modelling of air temperature in a mountainous region of Northern Spain. *Agricultural and forest meteorology*, 146(3-4):173–188, 2007.

James E. Bennett, Marta Blangiardo, Daniela Fecht, Paul Elliott, and Majid Ezzati. Vulnerability to the mortality effects of warm temperature in the districts of England and Wales. *Nature Climate Change*, 4:269–273, 2014. doi: 10.1038/nclimate2123.

Marta Blangiardo, Michela Cameletti, Gianluca Baio, and Håvard Rue. Spatial and spatio-temporal models with R-INLA. *Spatial and spatio-temporal epidemiology*, 4:33–49, 2013.

Melissa Blum, Donato DeIngeniis, Daniela K. Shill, Joanne Stone, Perry Sheffield, and Yoko Nomura. Association of early pregnancy warm season exposure and neighborhood heat vulnerability with adverse maternal outcomes: A retrospective cohort study. *The Journal of Climate Change and Health*, 25:100524, 2025. ISSN 2667-2782. doi: 10.1016/j.joclim.2025.100524.

Alfésio LF Braga, Antonella Zanobetti, and Joel Schwartz. The effect of weather on respiratory and cardiovascular deaths in 12 US cities. *Environmental health perspectives*, 110(9):859–863, 2002.

Michela Cameletti, Finn Lindgren, Daniel Simpson, and Håvard Rue. Spatio-temporal modeling of particulate matter concentration through the SPDE approach. *AStA Advances in Statistical Analysis*, 97:109–131, 2013.

Jorge Castillo-Mateo, Miguel Lafuente, Jesús Asín, Ana C. Cebrián, Alan E. Gelfand, and Jesús Abaurrea. Spatial modeling of day-within-year temperature time series: An examination of daily maximum temperatures in Aragón, Spain. *Journal of Agricultural, Biological and Environmental Statistics*, 27(3):487–505, 2022. doi: 10.1007/s13253-022-00493-3.

Jorge Castillo-Mateo, Jesús Asín, Ana C Cebrián, Alan E Gelfand, and Jesús Abaurrea. Spatial quantile autoregression for season within year daily maximum temperature data. *The Annals of Applied Statistics*, 17(3):2305–2325, 2023.

Emiliano Ceccarelli, Giada Minelli, Antonello Maruotti, Giovanna Jona Lasinio, and Marco Martuzzi. Understanding excess mortality in 2022: The dual impact of COVID-19 and heatwaves on the Italian elderly population. *Health & Place*, 90:103357, 2024.

Hayon Michelle Choi and Michelle L Bell. Heat-mortality relationship in North Carolina: Comparison using different exposure methods. *Journal of Exposure Science & Environmental Epidemiology*, 33(4):637–645, 2023.

Josh M Colston, Tahmeed Ahmed, Cloupas Mahopo, Gagandeep Kang, Margaret Kosek, Francisco de Sousa Junior, Prakash Sunder Shrestha, Erling Svensen, Ali Turab, Benjamin Zaitchik, et al. Evaluating meteorological data from weather stations, and from satellites and global models for a multi-site epidemiological study. *Environmental research*, 165:91–109, 2018.

CDS Copernicus Climate Change Service. ERA5 hourly data on pressure levels from 1940 to present, 2023.

Peter F Craigmile and Peter Guttorp. Space-time modelling of trends in temperature series. *Journal of Time Series Analysis*, 32(4):378–395, 2011.

F de’Donato, M Scorticichini, V Villani, P Mercogliano, M De Sario, M Davoli, P Michelozzi, et al. Future attributable deaths of heatwaves in Italian cities using high resolution climate change scenarios. *Environmental Epidemiology*, 3:357–358, 2019.

Dipartimento di Epidemiologia, Regione Lazio. Sistema di allerta per le ondate di calore. <https://deplazio.it/index.php/attivita/ambiente-e-salute/clima/ondate-di-calore>, 2025. Accessed: 2025-09-11.

Markus G Donat, Jana Sillmann, Simon Wild, Lisa V Alexander, Tanya Lippmann, and Francis W Zwiers. Consistency of temperature and precipitation extremes across various global gridded in situ and reanalysis datasets. *Journal of Climate*, 27(13):5019–5035, 2014.

Douglas Nychka, Reinhard Furrer, John Paige, and Stephan Sain. *fields: Tools for spatial data*, 2021. URL <https://github.com/dnnychka/fieldsRPackage>. R package version 16.3.

Fernando Ferraz Do Nascimento and Marcelo Bourguignon. Bayesian time-varying quantile regression to extremes. *Environmetrics*, 31(2):e2596, 2020.

Meng Gao and Christian LE Franzke. Quantile regression-based spatiotemporal analysis of extreme temperature change in China. *Journal of Climate*, 30(24):9897–9914, 2017.

Antonio Gasparini and Ben Armstrong. The impact of heat waves on mortality. *Epidemiology*, 22(1):68, January 2011. ISSN 1044-3983. doi: 10.1097/EDE.0b013e3181fdcd99.

Antonio Gasparini, Yuming Guo, Masahiro Hashizume, Eric Lavigne, Antonella Zanobetti, Joel Schwartz, Aurelio Tobias, Shilu Tong, Joacim Rocklöv, Bertil Forsberg, et al. Mortality risk attributable to high and low ambient temperature: a multicountry observational study. *The lancet*, 386(9991):369–375, 2015.

Robert M Gifford, Tommaso Todisco, Michael Stacey, Takeshi Fujisawa, Michael Allerhand, DR Woods, and RM Reynolds. Risk of heat illness in men and women: a systematic review and meta-analysis. *Environmental Research*, 171:24–35, 2019.

Yuming Guo, Antonio Gasparini, Ben G Armstrong, Benjawan Tawatsupa, Aurelio Tobias, Eric Lavigne, Micheline de Sousa Zanotti Staglorio Coelho, Xiaochuan Pan, Ho Kim, Masahiro Hashizume, et al. Heat wave and mortality: a multicountry, multicomunity study. *Environmental health perspectives*, 125(8):087006, 2017.

Jane L Harvill. Spatio-temporal processes. *Wiley interdisciplinary reviews: computational statistics*, 2(3):375–382, 2010.

Robert J. Hijmans. *terra: Spatial Data Analysis*, 2024. URL <https://CRAN.R-project.org/package=terra>. R package version 1.7-78.

Lily Hospers, Gabrielle A Dillon, Andrew J McLachlan, Lacy M Alexander, W Larry Kenney, Anthony Capon, Kristie L Ebi, Edward Ashworth, Ollie Jay, and Yorgi Mavros. The effect of prescription and over-the-counter medications on core temperature in adults during heat stress: a systematic review and meta-analysis. *EClinicalMedicine*, 77, 2024.

Holly Janes, Lianne Sheppard, and Thomas Lumley. Case-crossover analyses of air pollution exposure data: referent selection strategies and their implications for bias. *Epidemiology*, 16(6):717–726, 2005.

Giovanna Jona Lasinio, Gianluca Mastrantonio, and Alessio Pollice. Discussing the “big n problem”. *Statistical Methods & Applications*, 22:97–112, 2013.

Hanna Kaciuba-Uscilko and Ryszard Grucza. Gender differences in thermoregulation. *Current Opinion in Clinical Nutrition & Metabolic Care*, 4(6):533–536, 2001.

Cinoo Kang, Chaerin Park, Whanhee Lee, Nazife Pehlivan, Munjeong Choi, Jeongju Jang, and Ho Kim. Heatwave-related mortality risk and the risk-based definition of heat wave in South Korea: a nationwide time-series study for 2011–2017. *International journal of environmental research and public health*, 17(16):5720, 2020.

Glen P Kenny, Ronald J Sigal, and Ryan McGinn. Body temperature regulation in diabetes. *Temperature*, 3(1):119–145, 2016.

Roger Koenker. *Quantile regression*, volume 38. Cambridge university press, 2005.

Roger Koenker and Gilbert Bassett Jr. Regression quantiles. *Econometrica: journal of the Econometric Society*, pages 33–50, 1978.

Roger Koenker and Zhijie Xiao. Quantile autoregression. *Journal of the American statistical association*, 101(475): 980–990, 2006.

Garyfallos Konstantoudis, Cosesta Minelli, Ana Maria Vicedo-Cabrera, Joan Ballester, Antonio Gasparini, and Marta Blangiardo. Ambient heat exposure and COPD hospitalisations in England: a nationwide case-crossover study during 2007–2018. *Thorax*, 77(11):1098–1104, 2022.

Garyfallos Konstantoudis, Cosesta Minelli, Holly Ching Yu Lam, Elaine Fuentes, Joan Ballester, Bethan Davies, Ana Maria Vicedo-Cabrera, Antonio Gasparini, and Marta Blangiardo. Asthma hospitalisations and heat exposure in England: a case-crossover study during 2002–2019. *thorax*, 78(9):875–881, 2023.

Finn Lindgren and Håvard Rue. Bayesian spatial modelling with R-INLA. *Journal of Statistical Software*, 63(19):1–25, 2015.

Finn Lindgren, Håvard Rue, and Johan Lindström. An explicit link between Gaussian fields and Gaussian Markov random fields: the stochastic partial differential equation approach. *Journal of the Royal Statistical Society Series B: Statistical Methodology*, 73(4):423–498, 2011.

Jose Antonio Lopez-Bueno, Julio Diaz, F Follos, JM Vellón, MA Navas, Dante Culqui, MY Luna, G Sánchez-Martínez, and Cristina Linares. Evolution of the threshold temperature definition of a heat wave vs. evolution of the minimum mortality temperature: a case study in Spain during the 1983–2018 period. *Environmental Sciences Europe*, 33(1):101, 2021.

Yun Lu and Scott L Zeger. On the equivalence of case-crossover and time series methods in environmental epidemiology. *Biostatistics*, 8(2):337–344, 2007.

Malcolm MacLure. The case-crossover design: a method for studying transient effects on the risk of acute events. *American journal of epidemiology*, 133(2):144–153, 1991.

Thiago G Martins, Daniel Simpson, Finn Lindgren, and Håvard Rue. Bayesian computing with INLA: new features. *Computational Statistics & Data Analysis*, 67:68–83, 2013.

Barry McNicholl, Yee Hui Lee, Abraham G Campbell, and Soumyabrata Dev. Evaluating the reliability of air temperature from ERA5 reanalysis data. *IEEE Geoscience and Remote Sensing Letters*, 19:1–5, 2021.

Robert Mendelsohn, Pradeep Kurukulasuriya, Alan Basist, Felix Kogan, and Claude Williams. Climate analysis with satellite versus weather station data. *Climatic Change*, 81(1):71–83, 2007.

Paola Michelozzi, Daniela D’Ippoliti, Ursula Kirchmayer, Manuela De Sario, Claudia Marino, Francesca de’Donato, and Carlo A. Perucci. Health impacts of extreme weather/heat waves, 1990–2004. Technical report, Dipartimento di Epidemiologia del Servizio Sanitario Regionale del Lazio, 2004. URL [https://www.deplazio.net/en/reports/doc\\_download/43-health-impacts-of-extreme-weatherheat-waves-1990-2004](https://www.deplazio.net/en/reports/doc_download/43-health-impacts-of-extreme-weatherheat-waves-1990-2004). Accessed: 2025-05-13.

Paola Michelozzi, Gabriele Accetta, Manuela De Sario, Daniela D’Ippoliti, Claudia Marino, Michela Baccini, Annibale Biggeri, H Ross Anderson, Klea Katsouyanni, Ferran Ballester, et al. High temperature and hospitalizations for cardiovascular and respiratory causes in 12 European cities. *American journal of respiratory and critical care medicine*, 179(5):383–389, 2009.

Malcolm N Mistry, Rochelle Schneider, Pierre Masselot, Dominic Royé, Ben Armstrong, Jan Kyselỳ, Hans Orru, Francesco Sera, Shilu Tong, Éric Lavigne, et al. Comparison of weather station and climate reanalysis data for modelling temperature-related mortality. *Scientific reports*, 12(1):5178, 2022.

Joaquín Muñoz-Sabater, Emanuel Dutra, Anna Agustí-Panareda, Clément Albergel, Gabriele Arduini, Gianpaolo Balsamo, Souhail Boussetta, Margarita Choulga, Shaun Harrigan, Hans Hersbach, et al. ERA5-Land: A state-of-the-art global reanalysis dataset for land applications. *Earth system science data*, 13(9):4349–4383, 2021.

William Navidi and Eric Weinhandl. Risk set sampling for case-crossover designs. *Epidemiology*, 13(1):100–105, 2002.

S. E. Perkins and L. V. Alexander. On the measurement of heat waves. *Journal of Climate*, 26(13):4500–4517, 2013. doi: 10.1175/JCLI-D-12-00383.1.

R Core Team. *R: A Language and Environment for Statistical Computing*. R Foundation for Statistical Computing, Vienna, Austria, 2024. URL <https://www.R-project.org/>.

Abi I Riley, Marta Blangiardo, Frédéric B Piel, Andrew Beddows, Sean Beevers, Gary W Fuller, and Paul Agnew. A Bayesian multisource fusion model for spatiotemporal PM2.5 in an urban setting. *arXiv preprint arXiv:2506.10688*, 2025.

Peter J. Robinson. On the definition of a heat wave. *Journal of Applied Meteorology*, 40(4):762–775, 2001. doi: 10.1175/1520-0450(2001)040<0762:OTDOAH>2.0.CO;2.

Joacim Rocklov, Adrian G Barnett, and Alistair Woodward. On the estimation of heat-intensity and heat-duration effects in time series models of temperature-related mortality in stockholm, sweden. *Environmental Health*, 11(1):23, 2012.

Dominic Royé, Carmen Íñiguez, and Aurelio Tobías. Comparison of temperature–mortality associations using observed weather station and reanalysis data in 52 Spanish cities. *Environmental research*, 183:109237, 2020.

Håvard Rue, Sara Martino, and Nicolas Chopin. Approximate bayesian inference for latent gaussian models by using integrated nested Laplace approximations. *Journal of the Royal Statistical Society Series B: Statistical Methodology*, 71(2):319–392, 2009.

Rakefet Shafran-Nathan, Ilan Levy, Noam Levin, and David M Broday. Ecological bias in environmental health studies: the problem of aggregation of multiple data sources. *Air Quality, Atmosphere & Health*, 10(4):411–420, 2017.

Scott C Sheridan, Cameron C Lee, and Erik T Smith. A comparison between station observations and reanalysis data in the identification of extreme temperature events. *Geophysical Research Letters*, 47(15):e2020GL088120, 2020.

Nidhi Singh, Ashtyn Tracy Areal, Susanne Breitner, Siqi Zhang, Stefan Agewall, Tamara Schikowski, and Alexandra Schneider. Heat and cardiovascular mortality: an epidemiological perspective. *Circulation research*, 134(9):1098–1112, 2024.

Karthik Sriram, R. V. Ramamoorthi, and Pulak Ghosh. Posterior consistency of Bayesian quantile regression based on the misspecified asymmetric Laplace density. *Bayesian Analysis*, 8(2):479–504, 2013. doi: 10.1214/13-BA817.

Janet Van Niekerk, Elias Krainski, Denis Rustand, and Håvard Rue. A new avenue for Bayesian inference with INLA. *Computational Statistics & Data Analysis*, 181:107692, 2023.

Yvette Van Steen, Anna-Maria Ntarladima, Rick Grobbee, Derek Karssenberg, and Ilonca Vaartjes. Sex differences in mortality after heat waves: are elderly women at higher risk? *International archives of occupational and environmental health*, 92(1):37–48, 2019.

Jennifer Vanos, Gisel Guzman-Echavarria, Jane W Baldwin, Coen Bongers, Kristie L Ebi, and Ollie Jay. A physiological approach for assessing human survivability and liveability to heat in a changing climate. *Nature communications*, 14(1):7653, 2023.

Daniel J Vecellio, S Tony Wolf, Rachel M Cottle, and W Larry Kenney. Evaluating the 35C wet-bulb temperature adaptability threshold for young, healthy subjects (PSU HEAT project). *Journal of Applied Physiology*, 132(2):340–345, 2022.

Andrew Verdin, Balaji Rajagopalan, William Kleiber, and Richard W Katz. Coupled stochastic weather generation using spatial and generalized linear models. *Stochastic Environmental Research and Risk Assessment*, 29(2):347–356, 2015.

WHO. *World Health Statistics 2016 [OP]: monitoring health for the sustainable development goals (SDGs)*. World Health Organization, 2016.

Simon N Wood. Thin plate regression splines. *Journal of the Royal Statistical Society Series B: Statistical Methodology*, 65(1):95–114, 2003.

Zhiwei Xu, Gerard FitzGerald, Yuming Guo, Bin Jalaludin, and Shilu Tong. Impact of heatwave on mortality under different heatwave definitions: a systematic review and meta-analysis. *Environment international*, 89:193–203, 2016.

Keming Yu and Rana A. Moyeed. Bayesian quantile regression. *Statistics & Probability Letters*, 54(4):437–447, 2001. doi: 10.1016/S0167-7152(01)00124-9.

## A Additional tables

Spatiotemporal method	Temperature (°C)
Method 1: 0.5 GQRM	28.07
Method 2: GGPM	26.94
Method 3: ERA5-Land	24.82

Table 1: MMTs (°C) by spatiotemporal methods.